Tissue-resident T cell–derived cytokines eliminate herpes simplex virus-2–infected cells

Pavitra Roychoudhury,[1,2] David A. Swan,[1] Elizabeth Duke,[1,3] Lawrence Corey,[1,2,3,4] Jia Zhu,[1,2] Veronica Davé,[1,5]
Laura Richert Spuhler,[1] Jennifer M. Lund,[1,5] Martin Prlic,[1,5,6] and Joshua T. Schiffer[1,3,4]

[1]Vaccine and Infectious Disease Division, Fred Hutchinson Cancer Research Center, Seattle, Washington, USA. [2]Department of Laboratory Medicine and [3]Department of Medicine, University of Washington, Seattle, Washington, USA. [4]Clinical Research Division, Fred Hutchinson Cancer Research Center, Seattle, Washington, USA. [5]Department of Global Health and [6]Department of Immunology, University of Washington, Seattle, Washington, USA.

The mechanisms underlying rapid elimination of herpes simplex virus-2 (HSV-2) in the human genital tract despite low CD8^{+} and CD4^{+} tissue-resident T cell (Trm cell) density are unknown. We analyzed shedding episodes during chronic HSV-2 infection; viral clearance always predominated within 24 hours of detection even when viral load exceeded 1×10^7 HSV DNA copies, and surges in granzyme B and IFN-γ occurred within the early hours after reactivation and correlated with local viral load. We next developed an agent-based mathematical model of an HSV-2 genital ulcer to integrate mechanistic observations of Trm cells in in situ proliferation, trafficking, cytolytic effects, and cytokine alarm signaling from murine studies with viral kinetics, histopathology, and lesion size data from humans. A sufficiently high density of HSV-2–specific Trm cells predicted rapid elimination of infected cells, but our data suggest that such Trm cell densities are relatively uncommon in infected tissues. At lower, more commonly observed Trm cell densities, Trm cells must initiate a rapidly diffusing, polyfunctional cytokine response with activation of bystander T cells in order to eliminate a majority of infected cells and eradicate briskly spreading HSV-2 infection.

Introduction

CD8^{+} and CD4^{+} tissue-resident T cells (Trm cells) rapidly identify and control recurrent human viral infections within peripheral sites (1–11). Trm cells lodge preferentially at prior sites of pathogen replication without recirculating in blood and are differentiated from circulating memory T cells based on microanatomic localization, cell-surface markers, and transcriptional profile (5, 12–15). During herpes simplex virus-2 (HSV-2) infection in humans, CD8^{+} T cells with Trm cell characteristics cluster at the dermal-epidermal junction, where neuron endings release HSV-2 into the mucosa (9, 10, 16). The heterogeneous spatial aggregation of Trm cells in genital skin explains the considerable variability of HSV-2 severity, including episodes that are contained after a few hours of viral replication and those that persist for many days and cause symptomatic lesions (17–21).

Recent murine studies employing intravital imaging describe the extraordinary range of Trm cell control mechanisms in situ. In the absence of antigen, Trm cells efficiently survey previously infected tissues to recognize and eliminate infected cells during reinfection (1, 22). During this immunosurveillance phase, Trm cells express dendrite-like arms to contact a large number of potentially infected cells (1, 22) and remain in an activated state despite the absence of antigen-driven stimulus via the T cell receptor (8). Upon recognition of an infected cell, Trm cell motility is restricted and abundant local proliferation ensues (22). Trm cells then mediate efficient, contact-mediated apoptosis of infected cells by releasing perforin and granzyme B (23–25).

Upon activation, Trm cells induce a broad antiviral program consisting of cytokine release and resultant generalized local inflammation (1, 8). Cytokines, notably IFN-γ, may induce clearance of HSV-2 infection (26, 27) and render surrounding cells resistant to infection, even with unrelated pathogens (1). Chemokines such as CXCL9 and CXCL10 may draw local immune cells to infected sites (11, 28). Cytokines and chemokines diffuse rapidly, are efficiently internalized by their target cells (29), and exert paracrine effects upon cells that are not in direct contact with Trm cells.

Analysis of human biopsy specimens of HSV-2–infected tissues reveals high-density clusters of both CD8^{+} and CD4^{+} Trm cells in certain microregions, with low densities of Trm cells in others (20). Yet a majority of HSV-2 shedding episodes are eliminated within 6 to 24 hours (19, 21, 30). Because individual HSV-2 ulcers are small, this rapid peak in viral load is more likely due to an intense local immune response rather than target cell limitation (19, 30–32).

It is unknown how low numbers of Trm cells orchestrate elimination of infected cells so efficiently. Different mechanisms may mediate elimination of a few infected cells over hours during mild episodes versus thousands of infected cells over days during more severe episodes. Here, we construct an agent-based mathematical model to recapitulate the spatiotemporal dynamics underlying the

viral spread, cytokine expansion, and Trm cell–mediated containment of HSV-2 in genital tissues.

Results

Intense immune pressure within 24 hours of HSV-2 detection. A characteristic of HSV-2 shedding episodes in chronically infected persons is rapid viral expansion, followed by a slightly more protracted clearance phase (21, 33, 34). Although most episodes share this core feature, they vary in severity. Many asymptomatic episodes are cleared in 6 to 12 hours and peak at less than 10^4 HSV DNA copies. Other episodes exceed 10^7 HSV DNA copies and are associated with visible lesions and shedding over days to weeks (30, 35, 36). In episodes longer than 4 days, longevity is driven by a rebound of HSV after an initial phase of clearance, likely due to seeding of new ulcers in immunologically distinct microenvironments (19).

To approximate viral dynamics within single-infection microenvironments, we reanalyzed 83 episodes (655 total swabs from 20 subjects) from a data set in which study participants performed swabs every 6 hours over 60 days. We binned episodes by duration into short (<1 day), medium (1–2 days), and long (>2 days) (30) and identified brisk viral expansion with an early peak in all episodes, even those with high viral loads (Figure 1A). There was a wide distribution of viral loads of the first episode peak (Figure 1B), ranging from 2.2 to 7.9 $\log_{10}$ HSV DNA copies. Episodes were of variable duration, but elimination usually occurred in less than 48 hours, with a minority lasting over 100 hours (Figure 1C). Median time to the first viral load peak was 7 hours; all episodes reached their first peak within 20 hours (Figure 1D). Moderate correlations were noted between time to first peak and first peak viral load (Figure 1E) and time to first peak and duration (Figure 1F). Symptoms tended to occur during episodes with the highest first viral load peak (Figure 1B) and of the longest duration (Figure 1C). Within symptomatic episodes, symptoms usually coincided with the highest local viral loads (Figure 1A).

These results confirm that massive HSV-2 replication is a defining early feature of shedding episodes. However, immunologic responses predominate — usually within 10 hours of viral detection and always within 20 — and time of the initial peak predicts severity. Whether an episode progresses to high viral loads and days of shedding or rapid containment in the first several hours may depend on the intensity of the immune response during the early hours of reactivation.

Heterogeneous dispersion of CD8+ and CD4+ Trm cells in HSV-2–infected genital tissues. HSV-2 reactivates in specific microenvironments throughout the human genital tract because of random traveling of virions along highly arborized branches of peripheral neurons (37). We previously observed a fixed spatial metastructure of CD8+ and CD4+ T cell density in infected tissue, defined by dense clusters in some regions and low numbers in others (20). To characterize tissue microenvironments, we summarized Trm cell densities observed in 18 genital biopsy specimens (Figure 2A) performed at 2 and 8 weeks following lesion healing (we refer to all observed T cells as Trm cells, though it is possible that a minority are not truly resident). We divided each image into regions, with 100 cells per region (Figure 2, B and C) and calculated the ratio of Trm cells to epithelial cells (in situ

effector/target [E:T] ratio) for CD8+ Trm cells, CD4+ Trm cells, and both subsets combined.

We then created a rank-order distribution of all observed ratios (Figure 2D). For CD8+ Trm cells, the median E:T ratio in the 779 microregions was 0.01 (IQR, 0–0.05; range, 0–1.58). For CD4+ Trm cells, the median E:T ratio in the 779 microregions was 0 (IQR, 0–0.01; range, 0–0.29). CD8+ Trm cells outnumbered CD4+ Trm cells at both 2 and 8 weeks after lesion healing (Figure 2D). The median E:T ratio was 0.02 (IQR, 0–0.07; range, 0–3.4) for CD8+ and CD4+ Trm cells combined. CD8+, CD4+, and both classes of Trm cells were absent in 37.1%, 60.7%, and 29.8% of the microregions (E:T = 0), respectively.

E:T ratios for the 18 specimens ranged from 0.01 to 0.24 (median = 0.03) for CD8+ Trm cells and from 0 to 0.03 (median = 0.01) for CD4+ Trm cells. For each specimen, we fit an exponential model to the rank order curve and achieved close reproduction of the data (Figure 2D and Methods). The median exponential slopes of the rank order abundance curve for all T cells was –0.121 (range, –0.222 to –0.045). Exponential slopes were similar between CD4+ (median, –0.197; range, –1.072 to –0.114) and CD8+ (median, –0.216; range, –1.77 to –0.083) Trm cells and fell within a narrow range at both 2- and 8-week time points (Figure 2D), implying that an equivalent gradient between high and low Trm cell density regions is imprinted during chronic HSV-2 infection (Figure 2, A and D). Specimens with a higher proportion of microregions with E:T = 0 had lower overall E:T ratios (Figure 2E).

A mathematical model of HSV-2 replication and spread within a single ulcer. We next sought to explain how infected cells are eliminated quickly, given the low Trm cell densities commonly observed in infected samples. To approximate spatial conditions of a single-infection microenvironment, we developed a 2D stochastic, agent-based mathematical model. Our goal was to precisely link spatial heterogeneity of Trm cell density (Figure 2) with observed heterogeneity in shedding episode kinetics (Figure 1). We developed the model in an iterative fashion to limit required parameter fitting at each step.

First, we simulated HSV-2 replication and spread, assuming no Trm cell immunity (Figure 3A; see Methods for details and Supplemental Table 1 for model parameters; supplemental material available online with this article; https://doi.org/10.1172/JCI132583DS1), to recapitulate early HSV-2 shedding episode kinetics. The agent-based model assumes that HSV-2 replication occurs in a 2-stage process within an infected cell. Newly infected cells enter a preproductive phase, during which immediate-early and early viral proteins are expressed, but HSV DNA replication has yet to occur (38). After several hours, HSV DNA polymerase activity initiates, leading to production of infectious viral particles for approximately 20 hours until cell lysis and death (Figure 3A).

Human HSV-2 infection occurs within nucleated epithelial cells in genital skin or mucosa. The 3D anatomy of this tissue space consists of approximately 2 to 10 stacked epidermal cells between the surface of the skin and the dermal-epidermal junction where HSV-2 is released from nerve endings. For simplicity, our model is made of a 2D lattice consisting of tightly packed square cells with 8 potential cellular contacts at edges and corners: this assumption is in accordance with the arrangement of squamous epithelial cells within tissue. Many cells in the top lay-
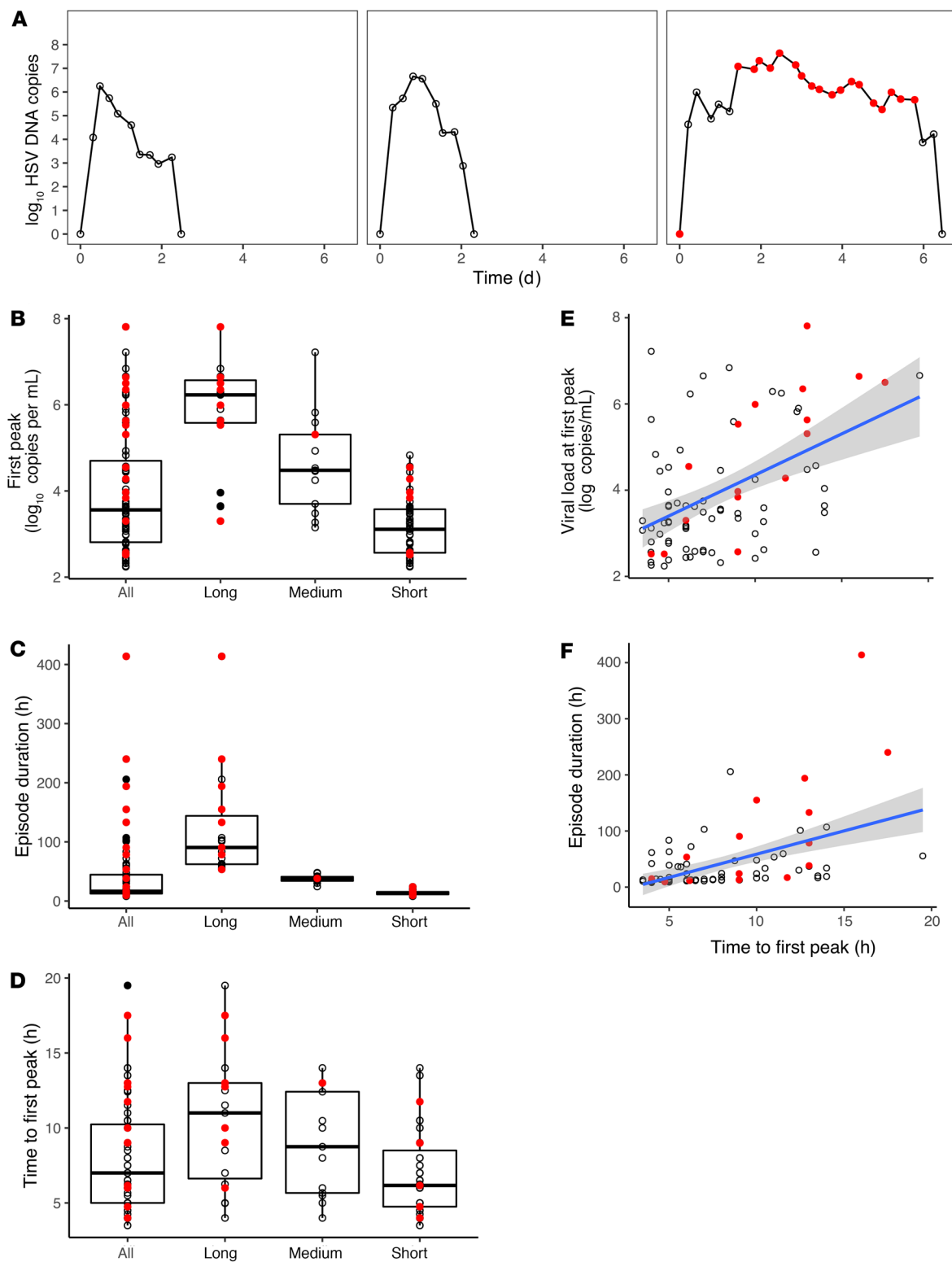
Figure 1. Early and intense immunological pressure against HSV-2 replication within genital microenvironments. (**A**) Three HSV-2 shedding episodes with typical characteristics, including rapid time to first peak viral load and rapid viral clearance. Red circles indicate symptomatic time points. (**B**–**D**) Analysis of 83 shedding episodes derived from every 6-hour genital sampling. Box plots with IQR (box) and 1.5 × IQR (whiskers). Categorization according to duration: short, under 24 hours (n = 51); medium, 24 to 48 hours (n = 13); and long, over 48 hours (n = 19). (**B**) Variable first peak viral loads and (**C**) durations across episodes, with most episodes eliminated in fewer than 48 hours. (**D**) Uniform occurrence of first peak viral load within the first 20 hours of HSV-2 detection. (**E**) Correlation of time to first peak viral load with peak episode viral load (Spearman's = 0.434, $P < 0.001$). (**F**) Correlation of time to first peak viral load with episode duration (Spearman's = 0.534, $P < 0.001$). (**B**–**F**) Red dots indicate symptomatic episodes, which tend to be longer and associated with higher first peak viral loads.
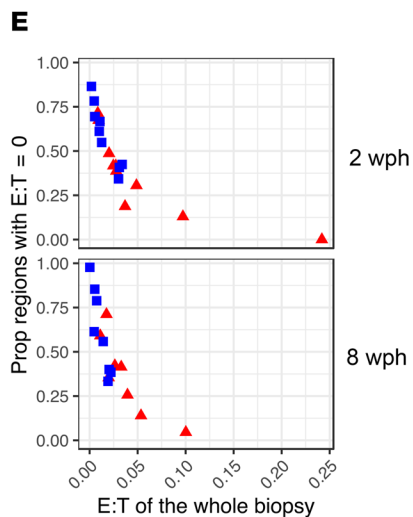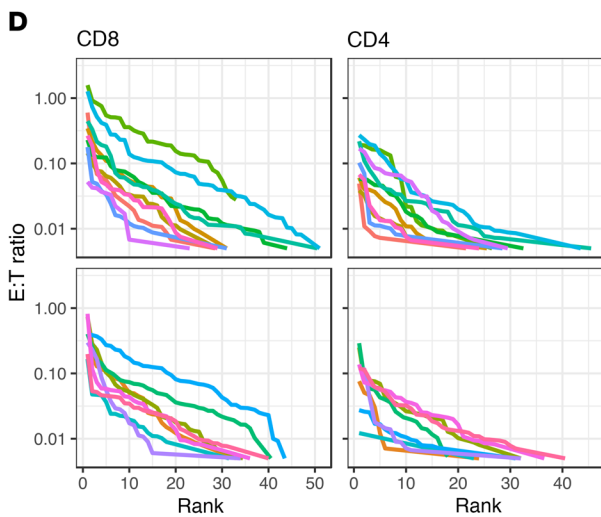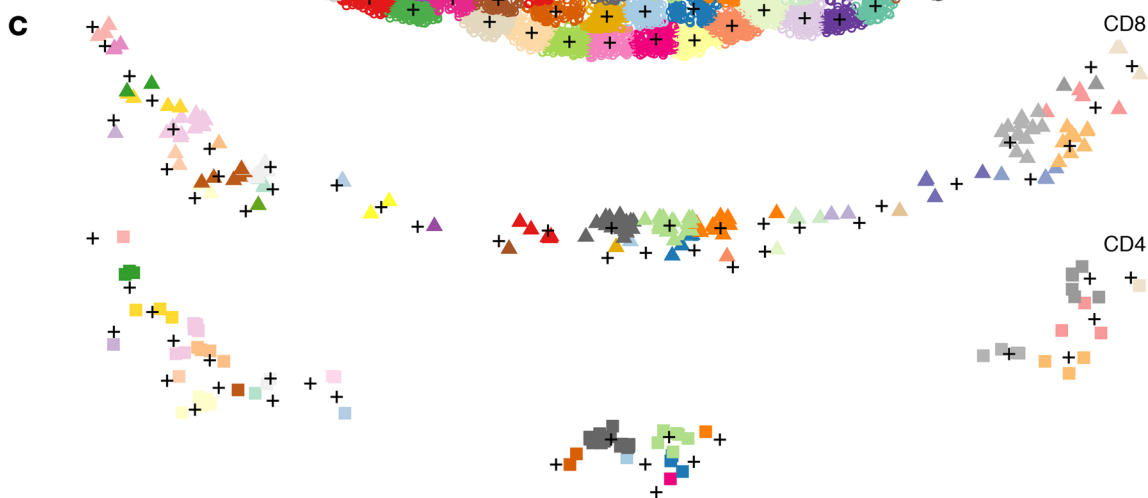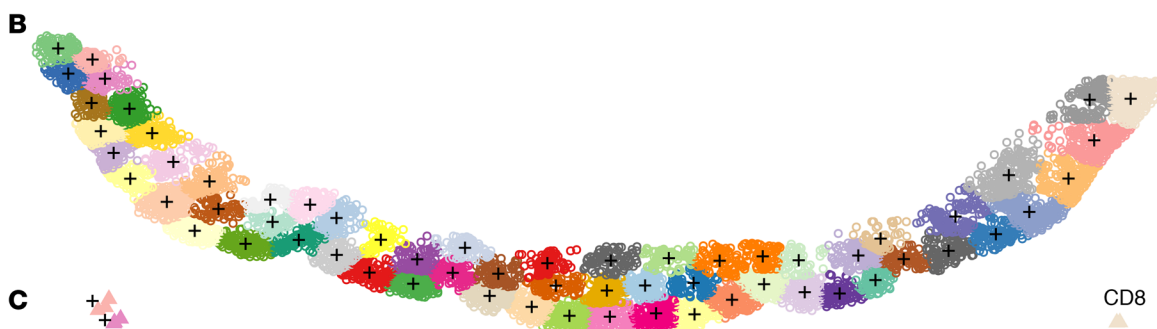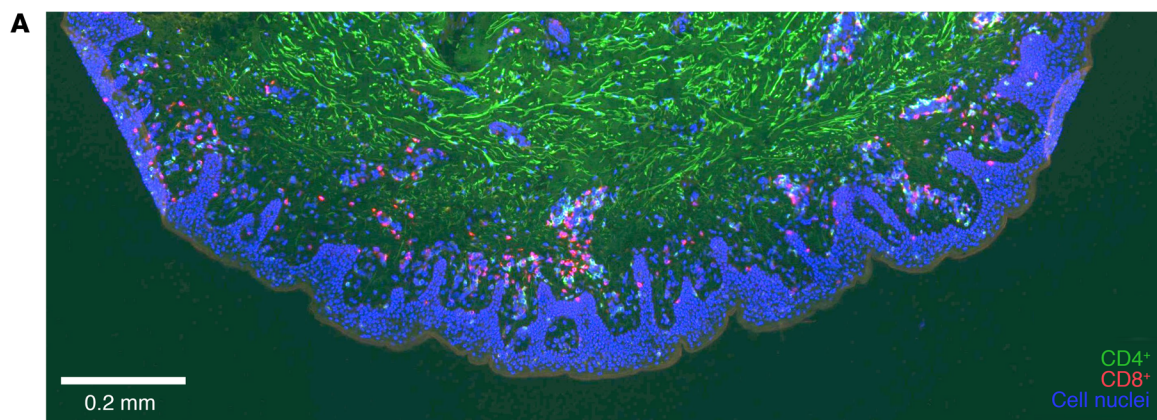
Figure 2. Heterogeneous dispersion of CD8+ T and CD4+ cells within HSV–2–infected genital biopsy specimens obtained after lesion healing. Analysis of 18 genital biopsy specimens from 10 participants 2 weeks (*n* = 9) or 8 weeks (*n* = 9) after lesion healing. (**A**) Three-color RGB image with cell nuclei (blue), CD4+ T cells (green), and CD8+ T cells (red) of a 2-week specimen. (**B**) 100-Cell microregions designated according to clusters shown as separate colors; +, cluster center. (**C**) CD8+ (triangles) and CD4+ T cells (squares) within each microregion. (**D**) Rank order distributions of effector/target (E:T) ratios within microregions. E:T ratios from each cluster are ranked according to size. Lines indicate single specimens; wide ranges of E:T ratios within each specimen indicate clustering of T cells in high-density regions and multiple regions with no T cells. Similar rank order slopes indicate a fixed gradient of T cell density across specimens (described in Results). (**E**) High variability of whole specimen E:T ratios (*x* axis) across 2- and 8-week specimens; inverse correlation of whole specimen E:T ratios with the proportion of 100 cell regions containing no CD8+ (red triangles) or CD4+ (blue squares) T cells (*y* axis).

ers of human skin are not permissive to HSV replication, so lateral cell-to-cell spread of HSV-2 is more efficient than apical-to-basal spread (39). Nevertheless, by neglecting the vertical dimension of cells, the model may underestimate total number of infected cells and viral load.

To approximate the observation that infection of adjacent cells occurs via tight junctions (40), we allowed individual viruses to diffuse with random directionality across the grid immediately after their production. Viruses that resided in the same model region as susceptible cells generated infection with a concentration-dependent probability at each time step (Methods).

Unimpeded HSV-2 spread in the absence of Trm cells. In simulations without Trm cells, viral load expanded rapidly during the first 12 to 18 hours of infection (Figure 3B) but reached maximal values slightly lower than those observed during the most severe shedding episodes (Figure 1, A and B). This discrepancy may be due to our model's 2D structure of cells. Another probable explanation is that the empirical data often include the sum of viral contributions from multiple ulcers, whereas we only model one ulcer (19).

In the absence of Trm cell activity, viral load did not peak but instead grew asymptotically with deceleration after 1 day (Figure 3B). Both total number of infected cells (Figure 3C) and ulcer diameter (Figure 3D) expanded. Realistic estimates of ulcer diameter (1–3 mm) were noted at 24 to 48 hours following infection, with large ulcers after several days (Figure 3D).

A 2D structure of uncontrolled infection emerged from the model (Supplemental Video 1). The leading edge of simulated ulcers consisted of preproductive, newly infected cells surrounding a thicker band of productively infected cells and a central core of dead and regenerating cells (Figure 4A). An outer ring of high viral load overlying productively infected cells was noted after 2 days (Figure 4B), with a far outer ring of lower viral load due to viral diffusion. The asymptotic behavior of viral load relates to spatial features of the mathematical model: target cell limitation increases with further expansion of the simulated ulcer. Specifically, as infection spreads radially, new infected cells are increasingly likely to contact already infected or dead cells (41).

Persistent high viral load shedding and large nonhealing ulcers are well-described features of infection in persons with severely compromised T cell immunity due to HIV/AIDS or stem cell transplantation (42). Our basic model recapitulates untreated HSV-2 infection in these clinical populations.

A mathematical model incorporating Trm cell trafficking, dendricity, local proliferation, and rapid contact-mediated killing of infected cells. Most immunocompetent persons start to clear each HSV-2 shedding episode within a day after viral load peaks (Figure 1). To capture this fact, we added Trm cell immunity to the baseline model (Methods and Supplemental Table 2). For each simulated episode, we generated varying realistic densities of CD8+ and CD4+ Trm cells across the modeled grid based on our analysis of biopsy specimens (Figure 2), by randomly sampling from exponential model reproductions of Trm cell abundance (Figure 2D and Methods). A relatively low percentage of CD8+ T cells from genital lesions (range, 1%–10%) were specific for HSV-2, though this was contingent upon recognition of a single preselected HLA-restricted HSV epitope (9, 43). These percentages are low bounds for the actual total percentages of CD8+ T cells that are specific to HSV-2, given that multiple HSV epitopes are likely to induce HSV-specific T cell responses. To represent conditions favoring the local immune system, we used a higher percentage (40%) of Trm cells retaining the ability to recognize HSV-2 antigen and kill adjacent infected cells in a contact-dependent manner.

Numerous recent murine studies allow parameterization of Trm cell behavior in tissue during the immunosurveillance phase between HSV-2 shedding episodes. When cognate antigen is not present, Trm cells patrol the cellular grid (Figure 5A and ref. 44). Recent evidence provides rates for Trm cell movement and suggests that trafficking follows a random walk over time scales of hours (1, 22). Patrolling Trm cells project dendritic arms to achieve a greater number of contacts with adjacent cells (Figure 5A and refs. 1, 22). We selected a value for Trm cell dendricity that captures the average number of target cells that a single Trm cell touches at a given point in time.

HSV-2–specific Trm cells undergo phenotypic changes upon contacting and engaging an infected cell, taking on a round morphology and transiently limited mobility. Brisk in situ Trm cell proliferation ensues; in the context of a significant peptide challenge, Trm cell levels increase approximately 10-fold over a 24-hour period in some models, though this is likely a high estimate (Figure 5A and refs. 23, 24). With the goal of again simulating conditions favoring local immunity, we included in situ proliferation at this high rate in our model.

Upon recognizing and adhering to an infected cell, Trm cells induce apoptosis within 30 minutes, presumably via secretion of granzyme B and perforin (Figure 5A and ref. 25). In our simulations, Trm cells occupy sites on the grid of epidermal cells. If Trm cells are at sites adjacent to (via a corner or edge) or in the same location as an infected cell, they can kill these infected cells via TCR contact–mediated mechanisms at a fixed rate or in a synergistic fashion, such that an infected cell contacted by several T cells dies more rapidly (Methods and ref. 25). We also assume that a single T cell can concurrently kill multiple adjacent infected cells via dendritic extensions (45). Cytokine paracrine effects against infected cells were not included in this version of the model.

Unimpeded HSV-2 spread in the presence of Trm cells that exert contact-mediated killing but no paracrine effects. When we simulated the model with the above assumptions of Trm cell immunosurveil-
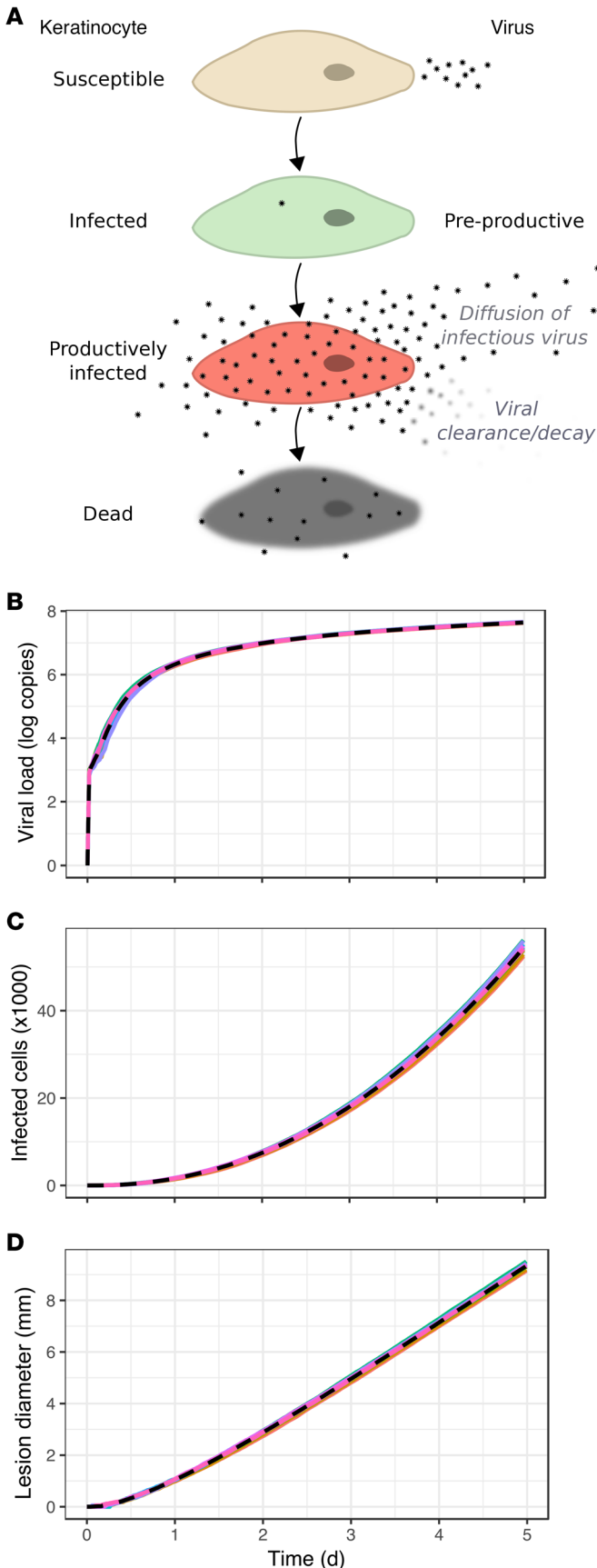
Figure 3. Continual expansion of HSV-2 infection in mathematical model simulations without Trm cells. (**A**) Mathematical model of HSV-2 replication and spread; infected cell progression through preproductive (green), and productive phases (red), during which viral replication occurs and virus diffuses to surrounding regions. (**B**) $\log_{10}$ HSV-2 viral load trajectory versus time for 10 simulated episodes with asymptotic behavior and no viral elimination (dotted line indicates median). (**C**) Number of infected cells and (**D**) ulcer diameter versus time with continual growth in the absence of a Trm cell response in the 10 simulated episodes.

lance and pathogen containment, there was insufficient immunologic pressure to eliminate all infected cells. We simulated 100 episodes at 10 realistic E:T ratios (range, 0.013–0.13). Asymptotic viral shedding was observed in all cases (Figure 5B). E:T ratio was predictive of viral load set point in these simulations (Figure 5C), indicating that contact-mediated killing by Trm cells exerts immunological pressure. We next simulated 100 episodes at extremely high E:T ratios (>0.20) rarely observed in our specimens (Figure 2E): only 21% were associated with viral elimination by 3 days, whereas the remaining episodes demonstrated persistent shedding at high viral copy number. We concluded that only very rarely does contact-mediated killing by Trm cells generate enough immunological pressure to achieve local viral containment.

A spatial approximation of this infection model demonstrates that more infected cells are killed by Trm cells than direct viral lysis (Supplemental Video 2 and Figure 6A) and that viral loads are lower per cellular region over time (Supplemental Video 2 and Figure 6B), relative to simulations without Trm cells (Supplemental Video 1 and Figure 4B). Nevertheless, HSV-2 spreads effectively through microregions of both low and high Trm cell density (Supplemental Video 3 and Figure 6C). We conclude that, despite the addition of multiple optimized Trm cell functions to our model, including highest possible rates of in situ killing, proliferation, and HSV-2 specificity, HSV-2 spread outpaces direct cell-to-cell killing via Trm cells and completely fails to recapitulate observed shedding episode features in immunocompetent humans (Figure 1A). This observation led us to include non–contact-mediated functions of Trm cells in our model.

Secretion of granzyme B and IFN-γ early during human HSV-2 shedding episodes. To validate inclusion of cytokines in our mathematical model, we performed local sampling for cytokine quantitation every 3 hours during naturally occurring shedding episodes in persons with chronic HSV-2 infection. During all episodes, we noted an early 1- to 2-log surge in granzyme B (Figure 7A), compatible with direct contact-mediated killing of infected cells by local T cells and NK cells. We detected an increase of similar magnitude in IFN-γ concordant with episode peaks (Figure 7A), suggesting that Trm cells exert paracrine effects. Because CD8^{+} and CD4^{+} T cells outnumber NK cells in HSV-2 lesions at the dermal-epidermal junction (16), these cells are likely to be critical producers of both detectable granzyme B and IFN-γ, though we cannot rule out contribution from NK cells in the dermis. Keratinocyte-derived cytokines, including IFN-α and IFN-β, did not consistently surge to comparably high levels during these episodes and were often absent or present at significantly lower levels (Figure 7A). Furthermore, across all samples (Figure 7B) and, in particular, in samples from the single largest lesion ulcer (Figure 7C), viral load

A Cells

B Virus
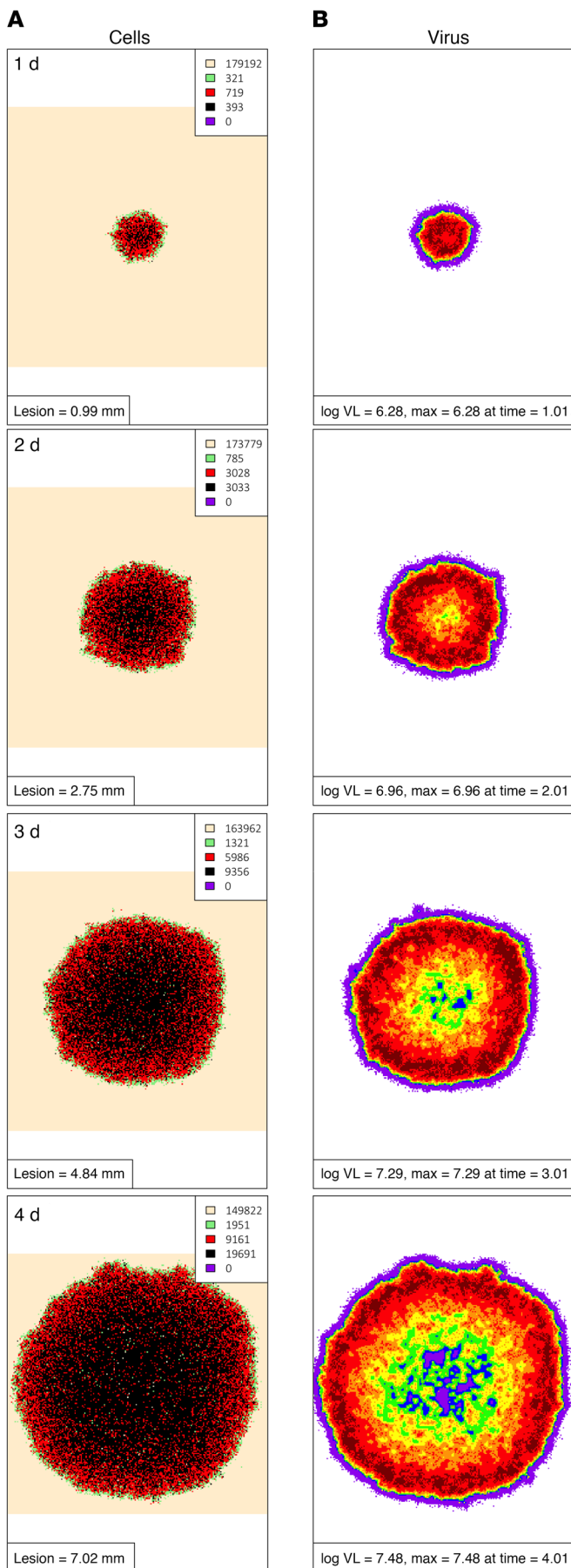
Figure 4. Continual spatial spread of HSV-2 infection in mathematical model simulations without Trm cells. Spatial approximation of infection spread in a 5-day simulation that corresponds to Supplemental Video 1 and Figure 3. One-day time steps per row starting at day 1. (**A**) An expanding ulcer with a leading edge of preproductively infected cells (green), an inner ring of productively infected cells (red), and a core of dead cells (black). Cell counts are shown in the inset. (**B**) Viral diffusion extending beyond the range of infected cells with highest local viral loads noted over regions with active HSV-2 replication; viral loads (HSV DNA copies) per cellular region: purple, 10^2–$10^{2.25}$; blue, $10^{2.25}$–$10^{2.5}$; green, $10^{2.5}$–$10^{2.75}$; yellow, $10^{2.75}$–10^3; orange, 10^3–$10^{3.25}$; red, $10^{3.25}$–$10^{3.5}$; dark red, >$10^{3.5}$.

showed a much stronger correlation with T cell–associated cytokines (granzyme B and IFN-γ) compared with epithelial-derived cytokines (IFN-α and IFN-β). Moreover, levels of granzyme B and IFN-γ were highly correlated, particularly from single-ulcer samples (Figure 7, B and C).

Model refinements to assess possible cytokine mechanisms for containment of local HSV-2 infection. Trm cell–secreted cytokines may generate a local alarm state via numerous paracrine mechanisms after diffusing across a field of cells. We updated our model to include 4 possible but unproven cytokine functions: (a) enhanced elimination of infected cells, (b) reduction in viral replication rate, (c) reduction in HSV-2 infectivity, and (d) induction of bystander (non–HSV specific) Trm cell proliferation and cytokine production (Figure 8A). Inclusion of these mechanisms as possibly relevant is experimentally justified based on in vitro and murine work: at minimum, the presence of IFN-γ is required for elimination of HSV spread and lowering viral titers in epithelial cells (26, 46); local production of IFN-γ has a powerful impact on gene expression within epithelial cells and other antigen-presenting cells (APCs) (47–49) and renders keratinocytes resistant to HSV-2 infection for several days in mice (2); Trm cell–derived cytokines, particularly IFN-γ, induce apoptosis in HSV-2–infected fibroblasts (27), though similar experiments in epithelial cells are lacking; finally, cytokines may stimulate proliferation, differentiation, and innate-like cytokine secretion from other local bystander CD8+ T cells in a paracrine fashion (49–53).

Because it is unknown which of these mechanisms is relevant during human infection, we generated 16 models with every possible combination, including a model lacking any cytokine functionality (Figure 5A) and one with all 4 functions. For all models, we assumed that bystander Trm cells are incapable of recognizing and lysing infected cells via direct contact. CD4+ T cells were included in the model, but assumed to lack direct killing ability based on lack of MHC-I expression, and therefore served as bystander cells that proliferate and contribute to the cytokine alarm system (53).

We imputed experimentally observed values of cytokine production by activated Trm cells into the model (Supplemental Table 3). The rate of cytokine diffusion across a cellular scaffold was estimated in vitro (29), and exceeded that of viral cell-to-cell spread. Given that rates of cellular uptake and diffusion of cytokines in vivo are unknown, we varied these 2 parameters across wide ranges of values for all models tested. For models including one or more of the mechanisms described above, we varied additional parameters. For instance, we included values
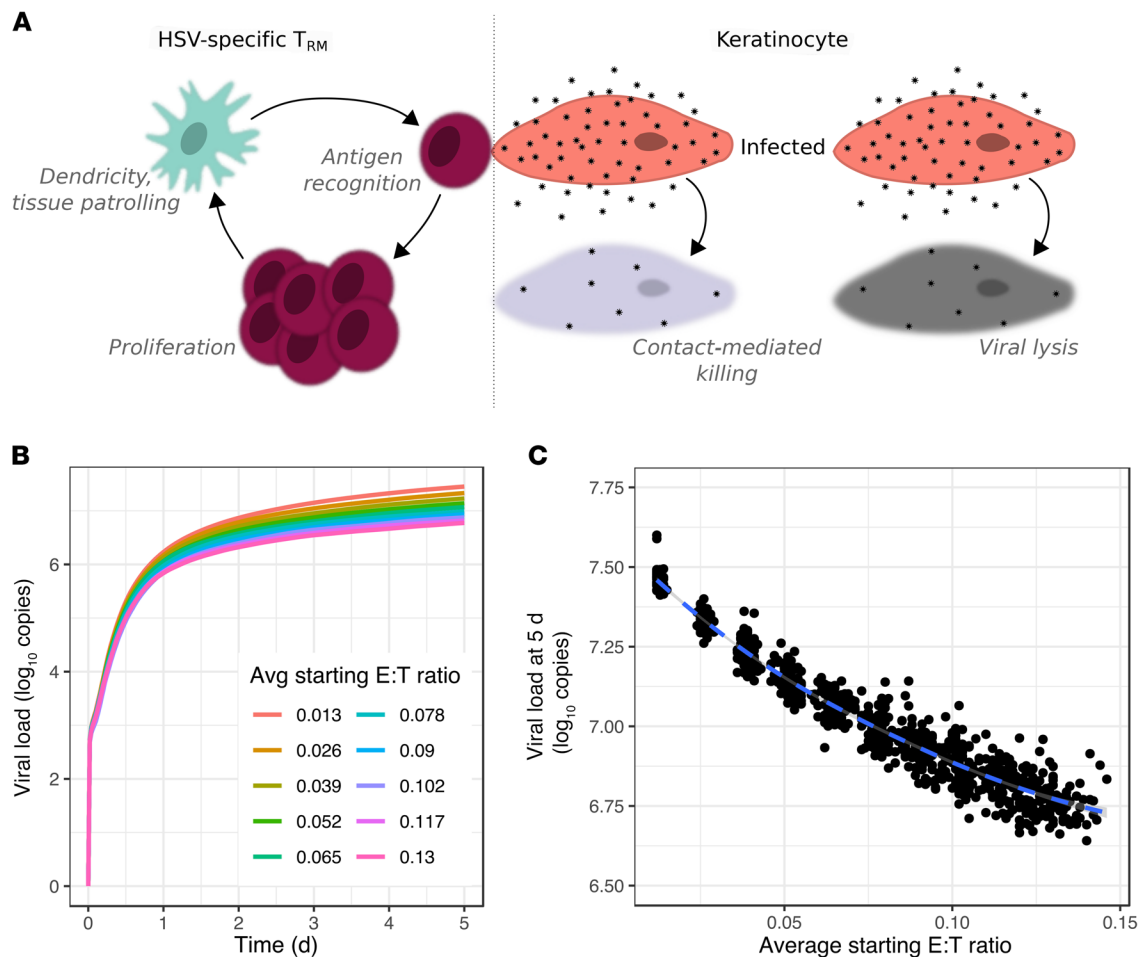
Figure 5. Failed elimination of infected cells in mathematical model simulations in which Trm cells only exert contact mediated killing. (**A**) Model schematic: between HSV-2 shedding episodes, Trm cell immunosurveillance by patrolling and expression of dendritic arms. During episodes, local Trm cell proliferation and killing of adjacent infected cells. (**B** and **C**) Simulated episodes at different E:T ratios. (**B**) Viral load trajectories with asymptotic behavior and lower set points at higher starting E:T ratios. (**C**) Inverse correlation between E:T ratio and viral load at day 5 (dot, 1 simulation; $n = 1000$).

to characterize the cytokine concentration at which a specific cytokine action was half-maximal in a given region.

We explored 500 possible randomly selected parameter sets for the 16 models. For each unique parameter set, we simulated 125 episodes, each with different initial conditions of Trm cell density drawn randomly from exponential models of rank-order distributions (Figure 2D). Given the stochastic nature of the model, we then used the best parameter set and performed 100 additional simulations to arrive at a range of model and parameter set–specific fitting scores. In total, we simulated 16,000,000 HSV-2 ulcers to identify an optimal model.

Recapitulation of shedding episode kinetics with incorporation of HSV-2–specific Trm cell cytokine secretion into the mathematical model. To identify which cytokine functions and parameters best recapitulate the observed data, we performed comparative model fitting to shedding episode data using Akaike information criteria (AIC) to reward for fit while penalizing for unnecessary complexity. We fit to shedding data from the 83 episodes described in Figure 1. Episodes were arrayed in rank abundance curves according to first peak viral load, duration, and time to first peak, such that the models were tasked with reproducing the entire distribution of shedding episode severity (Supplemental Figure 1). To mimic the

clinical protocol, we assumed sampling every 6 hours and random episode initiation 0 to 6 hours after each simulated sample.

Models with no cytokine activity fit poorly to the data, as virus was rarely eliminated (Figures 5 and 6 and Supplemental Figure 1A). Addition of a single cytokine mechanism improved fit only if the mechanism was increasing infected cell death rate or, to a lesser extent, lowering viral replication rate. Four models outperformed all other models by a significant degree, and each included a minimum of 2 cytokine mechanisms: increasing infected cell death rate and activation of bystander Trm cells (Figure 8A and Supplemental Figure 1A). A model with all 4 cytokine mechanisms gave the lowest median AIC scores over 100 runs; however, there was substantial run-to-run variability for a given model and parameter values due to the stochastic nature of the model (Supplemental Figure 1A). Based on overlapping AIC scores over 100 runs, decreased viral infectivity and lower HSV-2 replication rate cannot be formally ruled in or out as operative cytokine mechanisms during infection. Inclusion of these 2 mechanisms resulted in more realistically shaped round (rather than serpiginous) ulcers, and therefore they were kept in the model for all subsequent videos and figures.
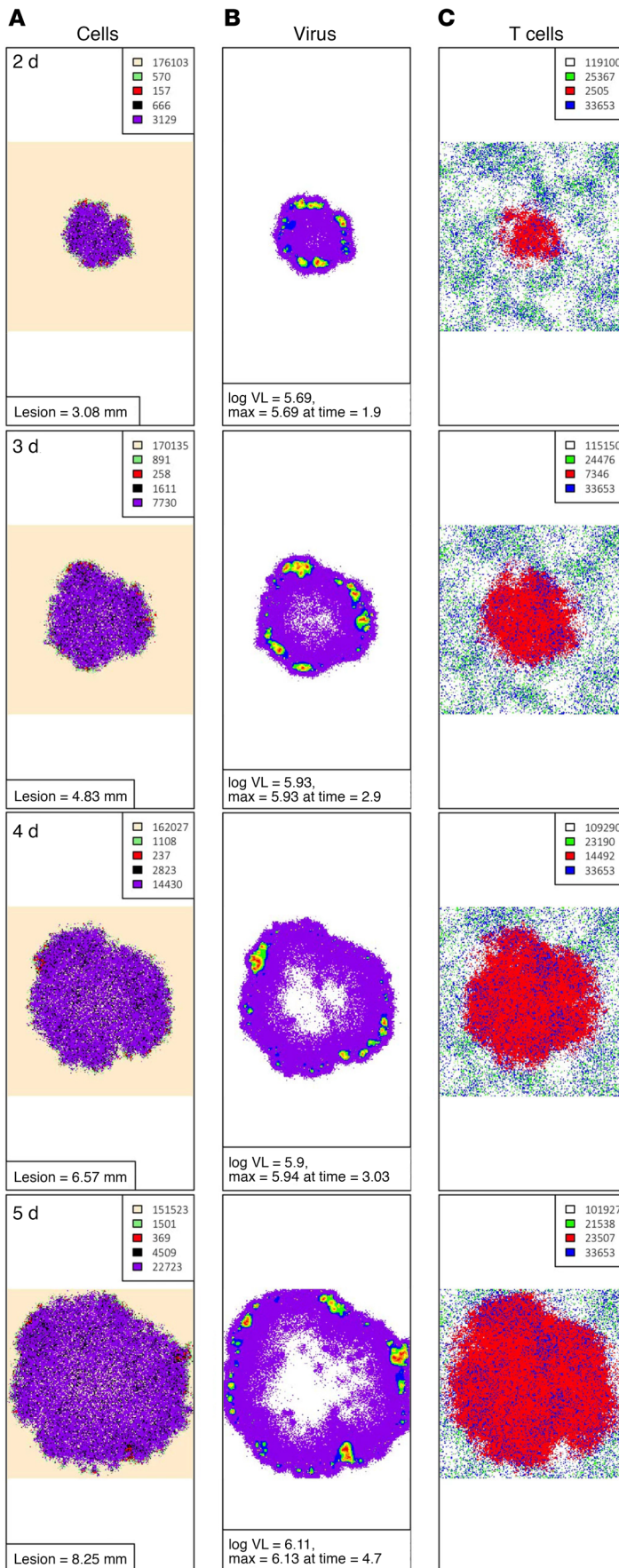
Figure 6. Failed elimination of viral spread in mathematical model simulations in which Trm cells only exert contact-mediated killing. Breakthrough spatial infection at a high E:T ratio (0.20) in a 5-day simulation that corresponds to Supplemental Video 2 and Figure 5. One-day time steps per row starting at day 2. (**A**) Preproductively infected cells (green) at the leading edge with a limited inner ring of productively infected cells (red), a core of virally lysed cells (black), and mostly Trm lysed cells (purple cells). Cell counts are shown in the inset. (**B**) Active HSV-2 replication within isolated intense foci of high local viral loads over regions with actively infected cells. Viral loads (HSV DNA copies) per cellular region: purple, 10^{2}–$10^{2.25}$; blue, $10^{2.25}$–$10^{2.5}$; green, $10^{2.5}$–$10^{2.75}$; yellow, $10^{2.75}$–10^{3}; orange, 10^{3}–$10^{3.25}$; red, $10^{3.25}$–$10^{3.5}$; dark red, >$10^{3.5}$. (**C**) HSV-2–specific Trm cell expansion during lesion spread (green, inactivated HSV-specific Trm cells; red, activated HSV-specific Trm cells; blue, inactivated bystander Trm cells). Cell counts are shown in the inset.

We added a fifth possible mechanism, cytokine induction of a chemical gradient to allow T cells to home to sites of infection; this did not alter the simulated data and was not subsequently included. Similarly, adjusting modes of Trm cell trafficking from random walk to Levy walk did not alter model fit and was not subsequently included. These results suggest that elimination of HSV-2–infected cells by cytokines involves at least 2 complementary mechanisms.

Finally, when we simulated the model with the assumption that only CD8+ Trm cells (and not CD4+ T cells, which lie deeper in the dermis) can contribute to local viral containment, we achieved only slightly worse median fit compared with the model inclusive of both cell populations (Supplemental Figure 1A). We are therefore unable to parse out the relative contributions of these 2 cellular populations.

The optimized model slightly overestimated distributions of episode first peak viral load and durations at moderate ranks (Supplemental Figure 1, B and C) and substantially underestimated first peak viral load and duration of the most severe episodes (Supplemental Figure 1, B and C) but closely recapitulated distribution of time to first episode peak (Supplemental Figure 1D). The model accepted a wide range of plausible values for rates of cytokine uptake into cells and viral diffusion. A narrower range was identified for cytokine diffusion rate, indicating the importance of this value for model fitting. Threshold upper limits were identified for necessary intracellular concentration of cytokines to limit viral replication and induce death in infected cells, prevent infection in uninfected cells, and activate surrounding Trm cells. These values were low, suggesting that cells are extremely sensitive to these proteins (Supplemental Table 3).

Rapid containment of infection under low Trm cell conditions due to rapid cytokine diffusion derived from HSV-2–specific Trm cells. Viral load trajectories in simulated episodes were notable for early peaks, rapid expansion rate, and short duration (Figure 8B); timing of cytokine surge (Figure 8B) was comparable to human shedding episodes (Figure 7A). As with murine studies (24), E:T ratio in the infected area was fairly predictive of first peak viral load in simulations; this was true when a field of 15,625 or 49 target cells was considered (Figure 8, C and D). A Trm cell–to–epithelial cell ratio of greater than 0.2
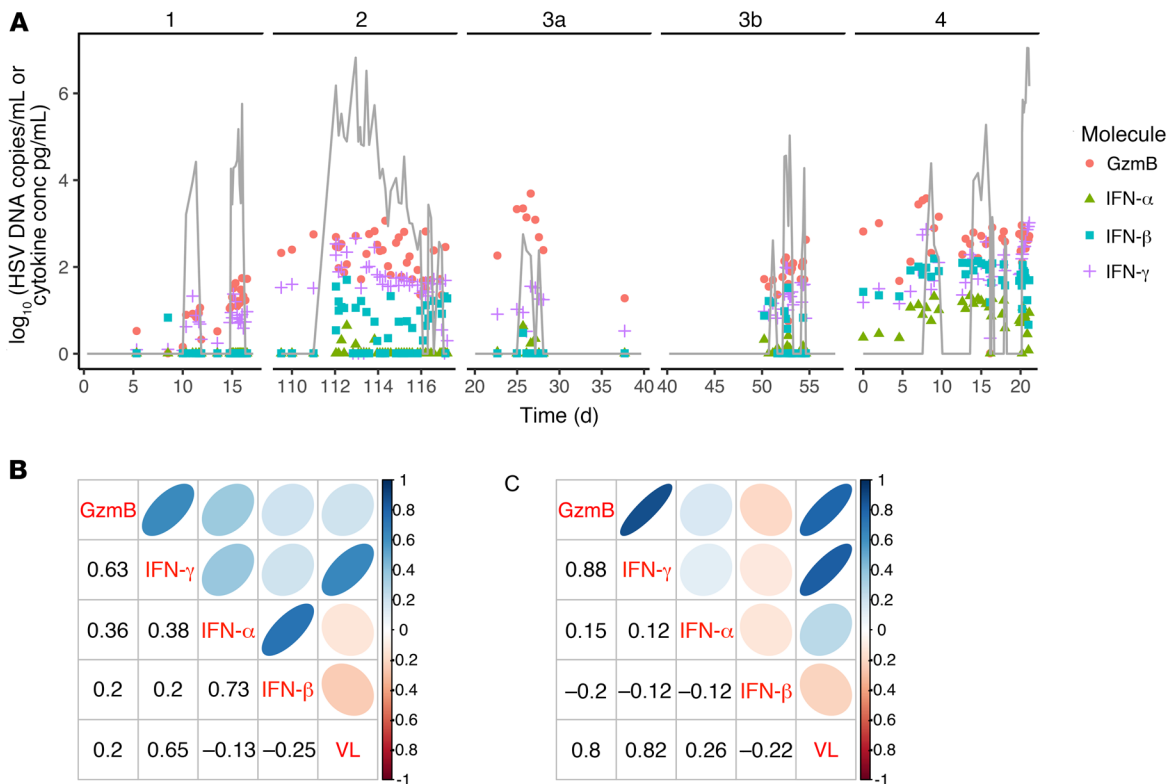
Figure 7. Trm cell–induced IFN-γ and granzyme B production during human HSV-2 shedding episodes. (A) HSV-2 shedding episodes and mucosal swab cytokine levels in 4 infected persons who swabbed every 8 hours before lesion detection and every 3 hours after lesion detection. HSV-2 DNA, gray line; copies/mL (*y* axis); granzyme B, pink circles; IFN-α, green triangles; IFN-β, blue squares; IFN-γ, purple crosses, all pg/mL (*y* axis). Values for both viral load and cytokines are log₁₀ converted. **(B and C)** Correlations between viral load (VL) and cytokine concentrations from pangenital swabs **(B)** and lesion-only swabs **(C)**. Numbers indicate Spearman's coefficients for a given pair aligned by columns and rows. Shapes are graphical representations of these values also aligned by columns and rows (blue, positive; red, negative; narrow and dark, high value; circular and light, low value). For instance, in **C**, the correlation between granzyme B and viral load is 0.8. Correlations among viral load, granzyme B, and IFN-γ are strong, while correlations with epithelial cell–derived IFN-α and IFN-β are weak or absent.

within the 49 target cell field was predictive of rapid elimination of HSV-2–infected cells before development of viral loads sufficient for lesion development and sexual transmission potential (>10⁴ HSV DNA copies) (Figure 8D); this exceeded ratios observed in most human biopsy specimens (Figure 2E). Early recognition of infection by Trm cells often resulted in elimination of virus in 6 to 24 hours with fewer than 20 total infected cells (Supplemental Video 4).

Spatial visualization demonstrates that, during more severe episodes, later initial recognition of an infected cell by an HSV-2–specific Trm cell (due to a lower Trm cell density) is followed by rapid diffusion of cytokines and immediate impact of cytokine antiviral effects (Figure 9 and Supplemental Videos 5 and 6). Accordingly, in simulations, both cellular distance between the initial infected cell and the nearest HSV-2–specific CD8⁺ T cell (Figure 10A) and time between infection of the first cell and recognition of an infected cell by an HSV-2–specific Trm cell (Figure 10B) were highly predictive of first peak viral load. Time to antigen recognition also was predictive of total number of infected cells (Figure 10C) and local shedding duration (Figure 10D). As episodes increased in severity, the proportion of infected cells killed by cytokine effects rather than direct lysis by Trm cells was generally higher (Figure 10E). For episodes contained to 5 or fewer cells,

100% were mediated by Trm cell–mediated contact killing alone without the need for cytokine functionality.

Trm cell density determines extent of episodes with higher numbers of initially infected cells. We previously demonstrated that prolonged episodes are likely due to sequential seeding of new ulcers in new microenvironments and that the cumulative viral load of severe episodes consists of viral production from numerous contemporaneous infection microenvironments (19). However, it is less certain whether the rapid wave of cytokines would limit additional viral production if multiple viral seeding events occurred within a single simulated microenvironment. To test for this effect, we simulated 1000 episodes with random selection of E:T ratio and varying numbers of initial numbers of infected cells within the 15,625 cells. Decreasing E:T ratios below 0.15 and, to a lesser extent, increasing the number of infectious plaques allowed higher first peak viral loads and numbers of infected cells (Supplemental Figure 2). This result may partially explain why our model fitting underestimated the highest viral load when starting with a single infected cell (Supplemental Figure 1B). However, viral seeding of immunologically distinct microenvironments, which occurs during human infection, is not captured in our model and is a more likely explanation for episodes extending beyond 3 days (Supplemental Figure 1C).
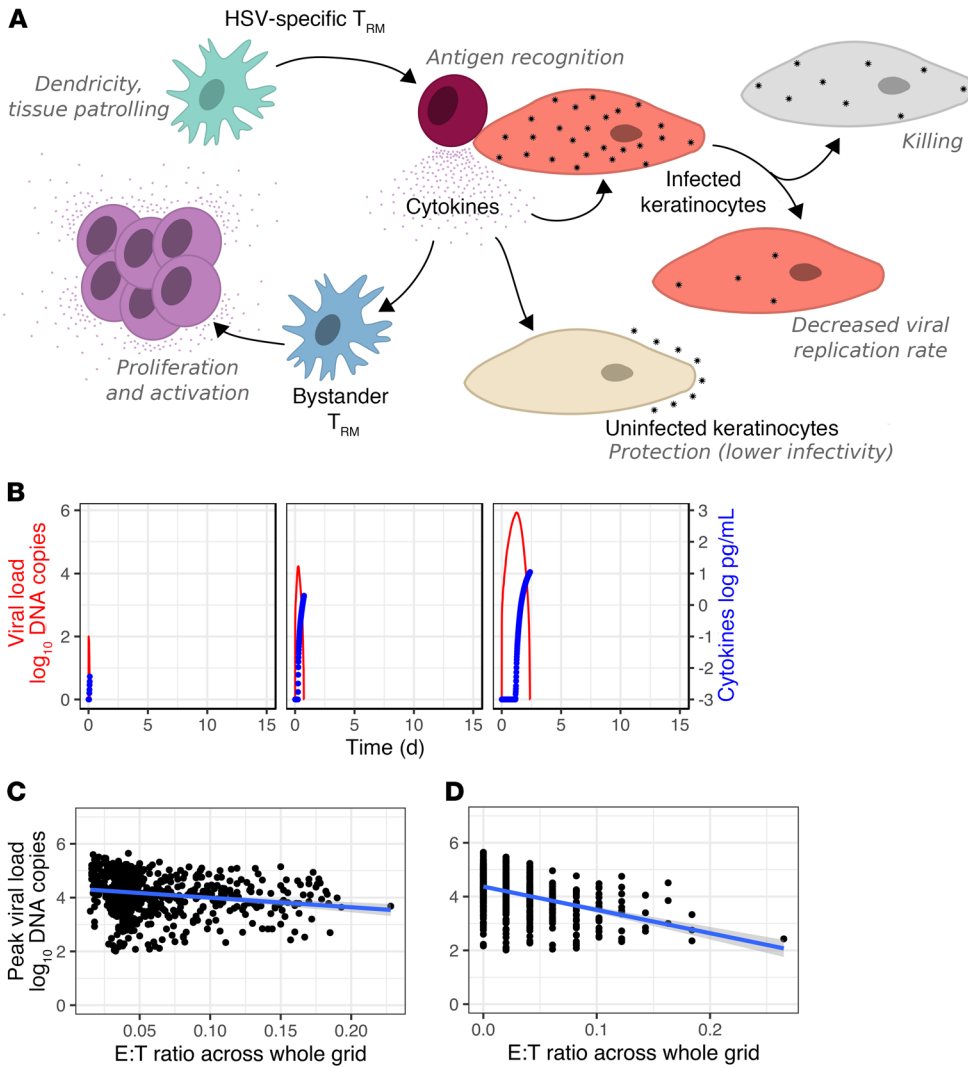
Figure 8. Mathematical models inclusive of multiple paracrine cytokine functions leading to realistic distributions of HSV-2 shedding episode severity. (**A**) Mathematical model schematic: possible cytokine effects including enhanced killing of infected cells, lowering viral replication rate in infected cells, lowering HSV-2 infectivity to uninfected cells, and activating other bystander Trm cells to proliferate and secrete cytokines; models including at minimum enhanced killing of infected cells and activation of other bystander Trm cells to proliferate and secrete cytokines provided best fit to the data (Supplemental Figure 1). (**B**) Three simulated episodes starting at different E:T ratios; $\log_{10}$ HSV-2 DNA (red) and relative cytokine concentration (blue). (**C** and **D**) 1000 Simulated episodes with starting E:T ratio densities (inclusive of CD4+ and CD8+ T cells) randomly selected from Figure 2D; inverse correlation of the ratio of Trm cells to epithelial cells within (**C**) the entire model grid of 15,625 cells and (**D**) the 49 cells surrounding the first infected cell to peak viral load. E:T ratio of greater than 0.2 immediately surrounding the first infected cell is most predictive of low peak viral load.

Polyfunctional and individually redundant antiviral cytokine effects within the HSV-2 infection microenvironment. To further delineate mechanisms of cytokine protection, we performed in silico knockout experiments by removing single and multiple cytokine mechanisms over 1000 sequential shedding episodes. These simulations demonstrated that elimination of single cytokine mechanisms generally had a limited effect on episode severity, yet when lowering infected cell life span and increasing bystander Trm cells were not assumed mechanisms in the model, a higher proportion of episodes had higher first peak viral loads (Supplemental Figure 3A), longer duration including persistence at 6 days (Supplemental Figure 3B), longer time to first peak viral load (Supplemental Figure 3C), and higher total number of infected cells (Supplemental Figure 3D). Among single cytokine mechanisms, activation of bystander Trm cells (particularly induction of cytokine secretion) and limitation of infected cell life span were most critical in limiting episode duration and time to first peak viral load. Simulations in which cytokines did not affect infected cell life span (Supplemental Video 7) or HSV infectivity (Supplemental Video 8) led to more protracted episodes in which ulcers took on an uncharacteristic serpiginous appearance.

Limited effects on HSV-2 elimination due to Trm cell trafficking, dendricity, proliferation, and cooperative killing. We performed additional in silico knockout experiments to identify the relative importance of non–cytokine-mediated Trm cell mechanisms of immune control. Surprisingly, elimination of Trm cell dendricity, mobility, or proliferation resulted in very little change in the overall proportion of episodes with higher first peak viral load (Supplemental Figure 4A), longer duration (Supplemental Figure 4B), longer time to first peak viral load (Supplemental Figure 4C), and total number of infected cells (Supplemental Figure 4D). Elimination of contact-mediated killing altogether also had only slight effects on these outcomes. However, reduction in the percentage of HSV-2–specific CD8+ Trm cells did allow more severe episodes overall (Supplemental Figure 4). This result implies that noncytokine Trm cell mechanisms such as proliferation and trafficking play a vital role in creating an optimal environment for immune surveillance between episodes but play less of a role in rapidly eliminating infected cells. The presence of virus-specific cells is vital for early episode recognition (Figure 8B).

T cell trafficking from blood is unlikely to explain observed HSV-2 shedding episode kinetics. In the murine system, within 72 hours of
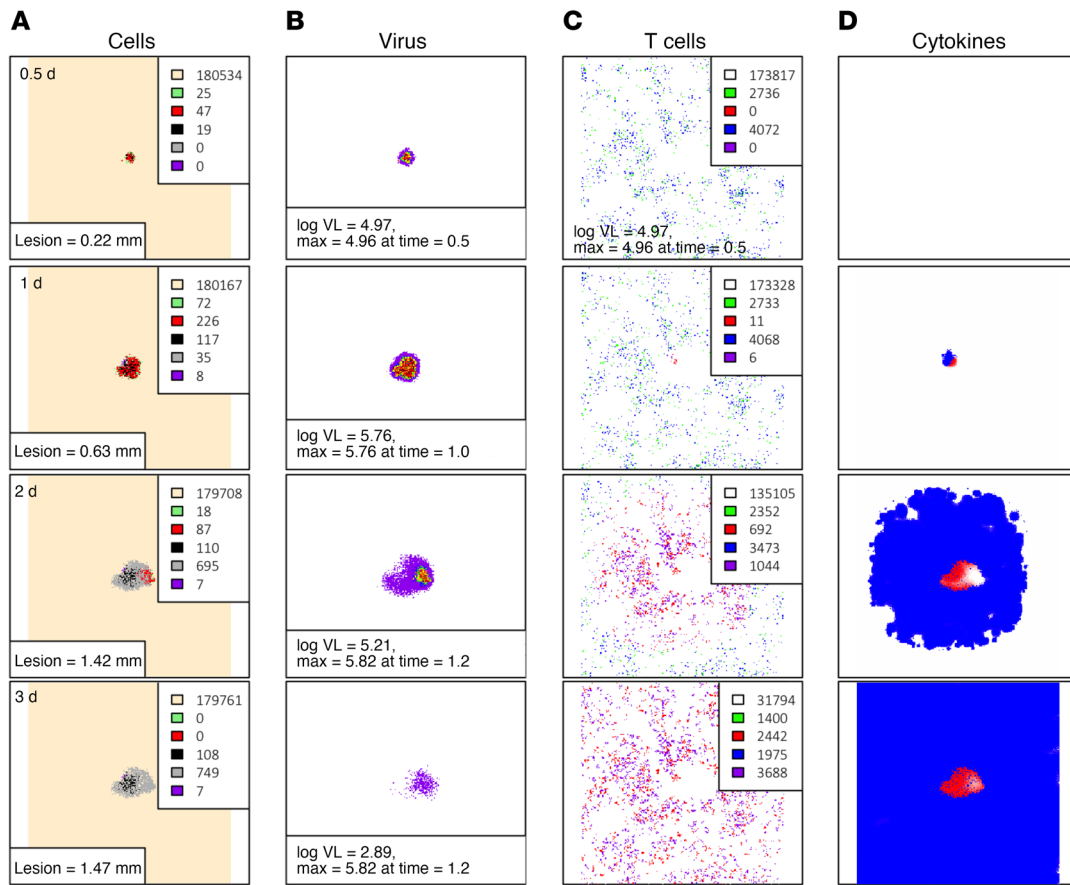
Figure 9. Cytokine diffusion leading to rapid elimination of infected HSV-2 cells. A simulated episode (corresponding to Supplemental Videos 5 and 6) with low Trm cell density leading to control of infection. Panels left to right: (**A**) Epidermal cell dynamics. Peach, uninfected; green, preproductive infection; red, productive infection; black, virally lysed cell; purple, Trm lysed cell; gray, cytokine lysed cell. Time steps for sampling are shown in the left upper corner; cell counts are shown in the inset. (**B**) Viral loads (HSV DNA copies) per cell: purple = 10^2–$10^{2.25}$, blue = $10^{2.25}$–$10^{2.5}$, green = $10^{2.5}$–$10^{2.75}$, yellow = $10^{2.75}$–10^3, orange = 10^3–$10^{3.25}$, red = $10^{3.25}$–$10^{3.5}$, dark red > $10^{3.5}$. (**C**) Trm cells, green, inactivated HSV-specific CD8+ Trm cells; red, activated HSV-specific CD8+ Trm cells; blue, inactivated bystander CD8+ or CD4+ Trm cells; purple, activated bystander CD8+ or CD4+ Trm cells. Cell counts are shown in the inset. (**D**) Concentration of cytokine by color darkness; red over infected or dead cells, indicating reduced infected cell lifespan; blue over uninfected cells, indicating reduced viral infectivity.

antigen introduction, local amplification of T cell levels is mainly via Trm cell proliferation rather than trafficking of CD8+ T cells from blood or draining lymph nodes (23, 24). In most cases of human infection, HSV-2 DNA has been eliminated from tissue at this (72- hour) time point. However, it is still possible that trafficking of effector memory T cells (Tem cells) contributes to local amplification of T cell levels soon after HSV-2 reactivation. Rapid production of proinflammatory cytokines and chemokines by epithelial cells has been shown to drive early T cell recruitment to infection sites (54).

We therefore tested the Tem cell mechanism in a model as an alternative to local Trm cell–mediated control. We assumed no Trm cells and estimated the number of HSV-2–specific T cells that would randomly passage through infected tissue per day by considering the following: the products of cardiac output, ratio of skin blood flow to total organ blood flow, ratio of genital skin to total skin, ratio of infected genital skin to total genital skin, lymphocytes per liter of blood, ratio of T cells to total lymphocytes, and ratio of HSV-2–specific T cells to total T cells in circulation (ref. 55 and Methods). Due to uncertainty and person-to-person variability in many of these values, we estimate that roughly 10

to 1000 HSV-2–specific Tem cells could arrive at a lesion per day. Although rapid trafficking of a high enough number of HSV-2–specific CD8+ T cells into infected tissue allowed for viral elimination, assuming cytokine production, this model did not produce the observed heterogeneity of episode first peak viral load, time to first peak viral load, and duration (Supplemental Figure 5), and AIC scores of the Tem cell model were well above those of the best Trm cell model. Therefore, heterogeneity in spatial density of Trm cells is a more likely explanation for the observed shedding episode data.

Discussion

Trm cells play a critical role in mucosal protection against HSV-2. During chronic infection, genital tissue contains HSV-2–specific CD4+ and CD8+ Trm cells months after local elimination of infected cells (9). The release of HSV-2 from latently infected ganglia via sensory neurons into genital tissues is temporally and spatially stochastic, resulting in seeding of low- and high-density Trm cell regions (19, 20, 56). Reactivations are initiated by infection of epithelial cells by ganglionic derived viruses, which are released from neurons in very low numbers based on the low replication rate of
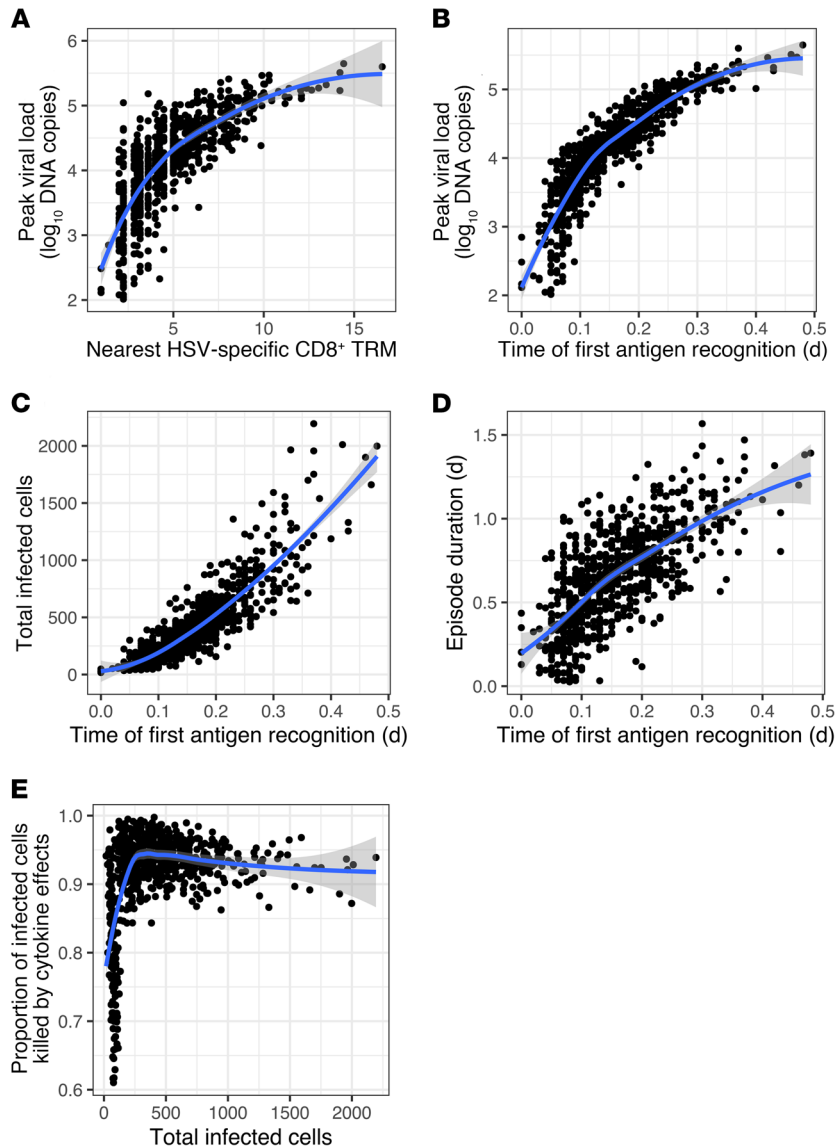
Figure 10. Time of HSV-2 recognition by HSV-2–specific Trm cells as a determinant of local infection severity. One thousand simulated episodes with initial E:T ratio densities randomly selected from exponential models of CD8+ and CD4+ Trm cell data shown in Figure 2D. (**A**) Correlation of cellular distance between nearest HSV-specific CD8+ Trm cells and first infected cell with $\log_{10}$ peak viral load. (**B–E**) Correlations of time to first Trm cell recognition of an infected cell with (**B**) $\log_{10}$ peak viral load, (**C**) total infected cells, and (**D**) duration. (**E**) Proportion of infected cells killed by cytokine effects as a function of number of total infected cells per episode. Of episodes, 20.5% involve only a single infected cell. Blue lines, LOESS-smoothed lines with 95% CI in gray.

the virus in neuron cell bodies (57). Previous data from our group indicate that, despite a slow, steady release of virus from the ganglia, initiation of infection within a single epithelial cell leading to detectable HSV-2 reactivation is likely a rare event (once per week in a typical infected person) (58). Following infection of a small number of epithelial cells, viral amplification and spread may then proceed rapidly. Within microregions, the spatial heterogeneity of Trm cells results in highly variable amounts of viral replication and subsequent Trm cell–mediated expansion (21). At the whole-tissue level, the result is a shedding pattern characterized by many brief episodes (approaching sterilizing immunity) in

which infection is limited to a few cells, but other episodes that persist for days and are associated with lesions, infection of thousands of epithelial cells, multiple loci of infection, and high transmission risk (59, 60).

Although HSV-2 achieves sufficient replication to induce a disease state in many infected people, we show here that the immune system wins each local battle with remarkable efficiency. Viral loads usually peak within 12 hours, and always within 24 hours, after viral DNA detection; the abrupt transition from viral expansion to contraction is associated with high levels of granzyme B and IFN-γ. Using a mathematical model, we demonstrate that during the critical early hours of reactivation when only a few cells are infected, if an HSV-2–specific Trm cell is in proximity, then it will induce rapid contact-mediated apoptosis and the episode will terminate without need for an amplified local response. If infection expands to hundreds or thousands of cells over 12 to 24 hours before Trm cell recognition and activation, then Trm cell contact–mediated killing is insufficient for pathogen control, despite efficient trafficking, expression of dendritic arms to canvas a high number of local cells, in situ proliferation, and rapid cooperative killing of infected cells.

The essential second step for truncating local shedding is cytokine secretion leading to a profound antiviral state. Secreted cytokines diffuse rapidly and are absorbed efficiently by infected keratinocytes (29). Based on best fit to observed data, our model suggests that cytokines exert at least 2 effects: rapid killing of infected cells and activation of bystander Trm cells, with possible lowering of HSV-2 replication rate and HSV-2 infectivity. Experimental evidence suggests that IFN-γ reduces HSV-2 infectivity to susceptible cells and may increase apoptosis of infected cells (26, 27). Inclusion of the latter mechanism was crucial for recapitulating early viral load peak and episode durations. Cytokines other than IFN-γ may be contributing to these effects in a synergistic matter. The rapid lethality of diffusing cytokines also explains the abrupt formation of clinical vesicles and erosions concurrent with viral clearance.

The generalized cytokine alarm state mechanism explains how HSV-2 elimination occurs rapidly within mucosal microregions defined by low HSV-specific Trm cell density (2). In our model, recognition of infected cells by a single pathogen-specific Trm cell is necessary but insufficient for initiation of tissue-wide protection. The timing of this sentinel event is the critical determinant of the extent of viral replication. We also demonstrate that episode heterogeneity is unlikely to be explained by a model in which infected cell elimination is governed primarily by circulating effector T cells. We previously demonstrated that local proliferation of Trm cells in response to HSV-2 reactivation, rather than

arrival of Tem cell from blood, is also the most likely explanation for the fixed spatial structure of these cells within infection microenvironments (20).

As was demonstrated in a mouse model, the total density of HSV-2–specific Trm cells is likely to be a key surrogate of immunity (24). In a 3 mm × 3 mm simulated microregion, and even more so within a smaller 50-cell region surrounding the first infected cell, Trm cell density maintains an inverse dose response with first peak viral load and shedding duration. Therefore, to achieve full protection, a therapeutic vaccine must achieve high HSV-2–specific Trm cell levels within all microregions across the genital region. During natural infection, the number of HSV-2–specific Trm cells is only sufficient to provide rapid protection in approximately 20% of tissue (20).

Our model projects that bystander Trm cells, which cannot recognize infected cells but secrete cytokines upon activation, play an important role in late elimination of infected cells during severe episodes. Removal of cytokine-mediated bystander Trm cell activation allows a higher proportion of uncontained episodes 6 days after initiation. However, a high density of Trm cells that lack antigenic specificity is not the most predictive surrogate of local immune protection. Rather, a sufficient number of HSV-2–specific CD8$^+$ Trm cells close to the site of reactivation is key for achieving near sterilizing immunity.

Our in silico knockout analysis allows a detailed assessment of the relative contribution of Trm cell phenotypic characteristics to the pace of HSV-2 elimination. Single noncytokine functions can be eliminated without dramatically impairing control of infection. Elimination of Trm cell trafficking, in situ proliferation, dendricity, or contact-mediated killing has only modest effects on viral load during simulations; however, deleting multiple functions leads to a slight increase in episode duration and first peak viral load. We conclude that most of these functions are vital for establishing an optimal environment for immunosurveillance between episodes.

Our approach has important limitations pertaining to oversimplification of the immune response. We cannot discriminate the relative per-cell potency of CD4$^+$ and CD8$^+$ Trm cell antiviral effects (28) and do not consider infiltrating NK cells. CD8$^+$ T cells colocalize with infected cells at the dermal-epidermal junction to a greater extent than CD4$^+$ T cells, which provide help at a distance from the dermis (16). We demonstrate that CD8$^+$ T cells are consistently present at higher numbers than CD4$^+$ T cells. NK cells lack antigen specificity and are present in lower abundance in healing genital specimens (8, 16). Nevertheless, both cell populations may be vital for early control of human herpes viruses, exhibit memory, and secrete IFN-γ, perforin, and granzyme B (10, 61, 62). Therefore, NK cells and CD4$^+$ Trm cells may serve as bystander cells and contribute to the alarm state (8). It will be important to distinguish the role of various infiltrating immune cell subsets in future models as relevant data accrues.

We also do not explicitly model cytokine-mediated epithelial cell–induced innate immunity (46, 63, 64), APCs (65), or antibody effects (66). Although these mechanisms undoubtedly play a role in pathogen elimination, their effects may not be as variably dispersed over time and tissue space as Trm cells. Unlike IFN-γ, keratinocyte-derived IFN-α and IFN-β levels were not correlated with local viral loads. Therefore, our model may capture humoral

and innate immunity effects that are embedded within static model parameters for viral replication, infectivity, and spread. In addition, we include a parameter to capture duration of T cell and infected cell contact required to induce Trm cell activation; this parameter indirectly captures the activity of APCs (67). If either of these effects vary in a nonlinear fashion relative to local viral load, or if infected epithelial cells and APCs sufficiently activate bystander Trm cells during severe episodes even in the absence of HSV-specific Trm cells, then our model misses these dynamics.

We denote cytokines as one variable in our model, which is overly reductionist. The multiple antiviral effects of IFN-γ are crucial, but a complex network of multiple cytokines is likely to influence HSV-2 containment, with varying effects according to cellular source and cellular target. Although a powerful cytokine impact on infected cells is a robust feature of our model, it currently lacks the granularity to distinguish effects of individual cytokines. A more comprehensive assessment will only be possible as new data allow detailed parameterization of individual cytokine effects on HSV-2–infected cell life span, viral replication, viral infectivity, and T cell bystander activation.

Finally, our model projections deviate from the observed data in important ways. The best-fitting model does not achieve the highest peak viral loads or durations observed in episodes, possibly because the 2D model includes fewer target cells for HSV-2 replication than human skin. Our model also only simulates a single ulcer, while swabbing protocols capture HSV-2 from multiple contemporaneous ulcers, particularly during severe high viral load episodes (19). Despite inclusion of multiple antiviral mechanisms, the optimal model slightly overestimated the distribution of episode first-peak viral loads and durations at low ranks. This may be because other infiltrating immune cell populations not included in the model contribute to control of infection. Another explanation is that our model assumes that all viruses being produced are detected with sampling, whereas in reality only cell-free viruses may be detected.

Despite these limitations, modeling provides a unique platform for linking observations from murine and human experiments, which is important because both of these approaches have inherent gaps. In humans, Trm cell responses evolve quickly within microscopic tissue environments and have not been captured during critical early stages of viral replication and spread. Successful containment of HSV-2 in a few cells is asymptomatic and even more difficult to observe empirically. Yet quantitative components of human data, including heterogeneity in shedding-episode kinetics and spatial density and topology of Trm cells, serve as critical benchmarks for model validation.

Murine models using intravital imaging allow observation and quantification of Trm cell behaviors. Indeed, these experiments inspired and informed our model (2). However, these experiments are rarely centered around realistic kinetics of pathogen control. Moreover, murine infection conditions may not be representative of human HSV-2 reactivation. It is plausible that Trm cell trafficking, dendricity, proliferation, synaptic killing, and antiviral cytokine release occur in humans and mice. Yet in vivo rates governing these behaviors may differ. Our analysis shows that knockout of some of these mechanisms results

in only small perturbations in viral shedding outcomes. As such, the models and results described here form the basis for hypotheses that may be confirmed through empirical observations from future human experiments.

Several experimental results in humans would strengthen the predictions of our model. For example, demonstration of strong upregulation of IFN-stimulated genes in uninfected cells and apoptotic signals in infected cells would be supportive. Single-cell transcriptomics may allow granular readouts of the source and impact of different cytokines expressed during and after contained local infection.

HSV-2–infected individuals experience shedding episodes that are frequent and highly variable due to the spatial distribution of Trm cells. We propose that containment of infection within low Trm cell–density areas is contingent upon rapid diffusion of antiviral cytokines from activated Trm cells. Effective vaccine strategies must increase the total number of HSV-2–specific Trm cells across the entire genital tract and leverage the broad protection afforded by antiviral cytokines to induce a spatially homogeneous layer of immunological readiness.

Methods

Study design. We reanalyzed data from a previous study where HSV-2 seropositive, HIV-negative individuals were asked to self-collect genital swab specimens 4 times a day for 60 days. Viral load was measured using quantitative PCR (qPCR) (30). For each participant, we divided the time series of viral loads into individual shedding episodes.

Image analysis of human biopsy specimens. We reanalyzed ×10 RGB images from previously described human HSV-2 genital biopsy specimens showing cell nuclei (blue), CD4+ T cells (green), and CD8+ T cells (red) (20). Each of 10 participants was biopsied at 2 and 8 weeks after healing of the lesions. Two samples were excluded because the neurons were too difficult to crop out. Using the 18 remaining images, we enumerated CD8+ and CD4+ T cells and total nuclei representative of T cells and epithelial cells using the program Cell Profiler (ref. 68 and Supplemental Methods).

Cytokine data from swabs. Four study participants with recurrent HSV lesions were enrolled in an additional protocol in which swabs were obtained every 8 hours before lesion development. At the time of prodrome or ulcer formation, participants switched to every 3 hour sampling for 5 days. Two swabs were obtained at each time point. One was processed for HSV PCR (36), and the other was sent for Meso Scale Discovery assay for cytokine quantitation (69). Data were analyzed as per sample (total genital tract viral loads, *n* = 326; lesion-only viral load, *n* = 185; total genital tract cytokines, *n* = 137; lesion-only cytokines, *n* = 112).

Individual-based model of viral spread and immunological containment of infection by Trm cells. We developed a stochastic, agent-based, spatially explicit model of HSV infection that incorporates key features of host and virus life cycles and immune control by CD8+ and CD4+ T cells, based on a previously developed model of host-pathogen dynamics (70). The model is described in detail in the Supplemental Methods.

Data and materials availability. All code and data are available at http://github.com/proychou/SpatialHSV (commit ID facf56bcd0d9d-8135e073c358342ebd3549c6d98). The model is available in both R and C++ versions and can be run on multiple computing platforms.

Statistics. For Figure 1, correlations were performed using Spearman's coefficient. For Figure 2, rank abundance curves were generated for projection of E:T ratios across microregions. Exponential model fitting to these distributions is described above. For Figure 5, correlations were performed between log-converted cytokine values and HSV-2 viral load using Spearman's coefficient. A *P* value of less than 0.05 was considered statistically significant.

Study approval. Data for these studies were obtained from a previous study where HSV-2–seropositive, HIV-negative individuals were asked to self-collect genital swab specimens (30). All study subjects gave informed consent before enrollment, and the human subjects protocols were approved by the University of Washington Institutional Review Board. All clinical investigations were conducted according to the principles expressed in the Declaration of Helsinki.

Author contributions

PR conceived the study, performed mathematical modeling, performed statistical analyses, and wrote the manuscript. DAS performed spatial analyses of biopsy specimens, mathematical modeling, and statistical analyses. ED assisted with literature review and model parameter selection. LC conceived the biopsy study. JZ performed staining of biopsy specimens. VD and LRS performed cytokine analysis. JML and MP conceived the study and edited the manuscript. JTS conceived the study, performed mathematical modeling, performed statistical analyses, and wrote the manuscript.

Address correspondence to: Joshua Schiffer, 1100 Eastlake Avenue East, Mailstop E4-100, Seattle, Washington 98109, USA. Phone: 206.667.7359; Email: jschiffe@fredhutch.org.

1. Ariotti S, et al. Tissue-resident memory CD8+ T cells continuously patrol skin epithelia to quickly recognize local antigen. *Proc Natl Acad Sci U S A*. 2012;109(48):19739–19744.
2. Ariotti S, et al. T cell memory. Skin-resident memory CD8+ T cells trigger a state of tissue-wide pathogen alert. *Science*. 2014;346(6205):101–105.
3. Gebhardt T, Palendira U, Tscharke DC, Bedoui S.

Tissue-resident memory T cells in tissue homeostasis, persistent infection, and cancer surveillance. *Immunol Rev*. 2018;283(1):54–76.
4. Gebhardt T, Wakim LM, Eidsmo L, Reading PC, Heath WR, Carbone FR. Memory T cells in nonlymphoid tissue that provide enhanced local immunity during infection with herpes simplex virus. *Nat Immunol*. 2009;10(5):524–530.

5. Mackay LK, et al. The developmental pathway for CD103(+)CD8+ tissue-resident memory T cells of skin. *Nat Immunol*. 2013;14(12):1294–1301.
6. Mackay LK, et al. Long-lived epithelial immunity by tissue-resident memory T (Trm) cells in the absence of persisting local antigen presentation. *Proc Natl Acad Sci U S A*. 2012;109(18):7037–7042.
7. Masopust D, Vezys V, Marzo AL, Lefrançois L.

Preferential localization of effector memory cells in nonlymphoid tissue. *Science*. 2001;291(5512):2413–2417.

8. Schenkel JM, Fraser KA, Beura LK, Pauken KE, Vezys V, Masopust D. T cell memory. Resident memory CD8 T cells trigger protective innate and adaptive immune responses. *Science*. 2014;346(6205):98–101.

9. Zhu J, et al. Virus-specific CD8+ T cells accumulate near sensory nerve endings in genital skin during subclinical HSV-2 reactivation. *J Exp Med*. 2007;204(3):595–603.

10. Zhu J, et al. Immune surveillance by CD8αα+ skin-resident T cells in human herpes virus infection. *Nature*. 2013;497(7450):494–497.

11. Shin H, Iwasaki A. A vaccine strategy that protects against genital herpes by establishing local memory T cells. *Nature*. 2012;491(7424):463–467.

12. Mackay LK, et al. Hobit and Blimp1 instruct a universal transcriptional program of tissue residency in lymphocytes. *Science*. 2016;352(6284):459–463.

13. Kumar BV, et al. Human tissue-resident memory T cells are defined by core transcriptional and functional signatures in lymphoid and mucosal sites. *Cell Rep*. 2017;20(12):2921–2934.

14. Sathaliyawala T, et al. Distribution and compartmentalization of human circulating and tissue-resident memory T cell subsets. *Immunity*. 2013;38(1):187–197.

15. Milner JJ, et al. Runx3 programs CD8+ T cell residency in non-lymphoid tissues and tumours. *Nature*. 2017;552(7684):253–257.

16. Zhu J, et al. Persistence of HIV-1 receptor-positive cells after HSV-2 reactivation is a potential mechanism for increased HIV-1 acquisition. *Nat Med*. 2009;15(8):886–892.

17. Schiffer JT. Mucosal HSV-2 specific CD8+ T-cells represent containment of prior viral shedding rather than a correlate of future protection. *Front Immunol*. 2013;4:209.

18. Schiffer JT, et al. Mucosal host immune response predicts the severity and duration of herpes simplex virus-2 genital tract shedding episodes. *Proc Natl Acad Sci U S A*. 2010;107(44):18973–18978.

19. Schiffer JT, et al. Rapid localized spread and immunologic containment define Herpes simplex virus-2 reactivation in the human genital tract. *Elife*. 2013;2:e00288.

20. Schiffer JT, et al. A fixed spatial structure of CD8+ T cells in tissue during chronic HSV-2 infection. *J Immunol*. 2018;201(5):1522–1535.

21. Schiffer JT, Wald A, Selke S, Corey L, Magaret A. The kinetics of mucosal herpes simplex virus-2 infection in humans: evidence for rapid viral-host interactions. *J Infect Dis*. 2011;204(4):554–561.

22. Zaid A, et al. Persistence of skin-resident memory T cells within an epidermal niche. *Proc Natl Acad Sci U S A*. 2014;111(14):5307–5312.

23. Beura LK, et al. Intravital mucosal imaging of CD8+ resident memory T cells shows tissue-autonomous recall responses that amplify secondary memory. *Nat Immunol*. 2018;19(2):173–182.

24. Park SL, et al. Local proliferation maintains a stable pool of tissue-resident memory T cells after antiviral recall responses. *Nat Immunol*. 2018;19(2):183–191.

25. Halle S, et al. In vivo killing capacity of cytotoxic T cells is limited and involves dynamic interactions and T cell cooperativity. *Immunity*. 2016;44(2):233–245.

26. Dobbs ME, Strasser JE, Chu CF, Chalk C, Milligan GN. Clearance of herpes simplex virus type 2 by CD8+ T cells requires gamma interferon and either perforin- or Fas-mediated cytolytic mechanisms. *J Virol*. 2005;79(23):14546–14554.

27. Peng T, Zhu J, Hwangbo Y, Corey L, Bumgarner RE. Independent and cooperative antiviral actions of beta interferon and gamma interferon against herpes simplex virus replication in primary human fibroblasts. *J Virol*. 2008;82(4):1934–1945.

28. Iijima N, Iwasaki A. T cell memory. A local macrophage chemokine network sustains protective tissue-resident memory CD4 T cells. *Science*. 2014;346(6205):93–98.

29. Thurley K, Gerecht D, Friedmann E, Höfer T. Three-dimensional gradients of cytokine signaling between T cells. *PLoS Comput Biol*. 2015;11(4):e1004206.

30. Mark KE, et al. Rapidly cleared episodes of herpes simplex virus reactivation in immunocompetent adults. *J Infect Dis*. 2008;198(8):1141–1149.

31. Corey L, Holmes KK. Genital herpes simplex virus infections: current concepts in diagnosis, therapy, and prevention. *Ann Intern Med*. 1983;98(6):973–983.

32. Mark KE, et al. Rapidly cleared episodes of oral and anogenital herpes simplex virus shedding in HIV-infected adults. *J Acquir Immune Defic Syndr*. 2010;54(5):482–488.

33. Schiffer JT, Magaret A, Selke S, Corey L, Wald A. Detailed analysis of mucosal herpes simplex virus-2 replication kinetics with and without antiviral therapy. *J Antimicrob Chemother*. 2011;66(11):2593–2600.

34. Schiffer JT, et al. Mathematical modeling of herpes simplex virus-2 suppression with pritelivir predicts trial outcomes. *Sci Transl Med*. 2016;8(324):324ra15.

35. Wald A, Zeh J, Selke S, Warren T, Ashley R, Corey L. Genital shedding of herpes simplex virus among men. *J Infect Dis*. 2002;186(suppl 1):S34–S39.

36. Wald A, et al. Reactivation of genital herpes simplex virus type 2 infection in asymptomatic seropositive persons. *N Engl J Med*. 2000;342(12):844–850.

37. Johnston C, et al. Virologic and immunologic evidence of multifocal genital herpes simplex virus 2 infection. *J Virol*. 2014;88(9):4921–4931.

38. Roizman BN, Knipe DM, Whitley RJ. Herpes Simplex Viruses. In: Knipe DM, Howley PM, eds. *Fields' Virology*. Philadelphia, Pennsylvania, USA: Lippincott-Williams and Wilkins; 2007:2501–2601.

39. Galen B, Cheshenko N, Tuyama A, Ramratnam B, Herold BC. Access to nectin favors herpes simplex virus infection at the apical surface of polarized human epithelial cells. *J Virol*. 2006;80(24):12209–12218.

40. Carmichael JC, Yokota H, Craven RC, Schmitt A, Wills JW. The HSV-1 mechanisms of cell-to-cell spread and fusion are critically dependent on host PTP1B. *PLoS Pathog*. 2018;14(5):e1007054.

41. Bauer AL, Beauchemin CA, Perelson AS. Agent-based modeling of host-pathogen systems: The successes and challenges. *Inf Sci (N Y)*. 2009;179(10):1379–1389.

42. Schiffer JT, Swan DA, Magaret A, Schacker TW, Wald A, Corey L. Mathematical modeling predicts that increased HSV-2 shedding in HIV-1 infected persons is due to poor immunologic control in ganglia and genital mucosa. *PLoS ONE*. 2016;11(6):e0155124.

43. Posavad CM, et al. Enrichment of herpes simplex virus type 2 (HSV-2) reactive mucosal T cells in the human female genital tract. *Mucosal Immunol*. 2017;10(5):1259–1269.

44. Fricke GM, Letendre KA, Moses ME, Cannon JL. Persistence and adaptation in immunity: T cells balance the extent and thoroughness of search. *PLoS Comput Biol*. 2016;12(3):e1004818.

45. Choi PJ, Mitchison TJ. Imaging burst kinetics and spatial coordination during serial killing by single natural killer cells. *Proc Natl Acad Sci U S A*. 2013;110(16):6488–6493.

46. Mikloska Z, Cunningham AL. Alpha and gamma interferons inhibit herpes simplex virus type 1 infection and spread in epidermal cells after axonal transmission. *J Virol*. 2001;75(23):11821–11826.

47. Saunders NA, Jetten AM. Control of growth regulatory and differentiation-specific genes in human epidermal keratinocytes by interferon gamma. Antagonism by retinoic acid and transforming growth factor beta 1. *J Biol Chem*. 1994;269(3):2016–2022.

48. Sanderson NS, et al. Cytotoxic immunological synapses do not restrict the action of interferon-γ to antigenic target cells. *Proc Natl Acad Sci U S A*. 2012;109(20):7835–7840.

49. Bhat P, Leggatt G, Waterhouse N, Frazer IH. Interferon-γ derived from cytotoxic lymphocytes directly enhances their motility and cytotoxicity. *Cell Death Dis*. 2017;8(6):e2836.

50. Whitmire JK, Tan JT, Whitton JL. Interferon-gamma acts directly on CD8+ T cells to increase their abundance during virus infection. *J Exp Med*. 2005;201(7):1053–1059.

51. Curtsinger JM, Agarwal P, Lins DC, Mescher MF. Autocrine IFN-γ promotes naive CD8 T cell differentiation and synergizes with IFN-α to stimulate strong function. *J Immunol*. 2012;189(2):659–668.

52. Tewari K, Nakayama Y, Suresh M. Role of direct effects of IFN-gamma on T cells in the regulation of CD8 T cell homeostasis. *J Immunol*. 2007;179(4):2115–2125.

53. Chu T, et al. Bystander-activated memory CD8 T cells control early pathogen load in an innate-like, NKG2D-dependent manner. *Cell Rep*. 2013;3(3):701–708.

54. Iversen MB, et al. An innate antiviral pathway acting before interferons at epithelial surfaces. *Nat Immunol*. 2016;17(2):150–158.

55. Moss NJ, et al. Peripheral blood CD4 T-cell and plasmacytoid dendritic cell (pDC) reactivity to herpes simplex virus 2 and pDC number do not correlate with the clinical or virologic severity of recurrent genital herpes. *J Virol*. 2012;86(18):9952–9963.

56. Schiffer JT, Swan DA, Prlic M, Lund JM. Herpes simplex virus-2 dynamics as a probe to measure the extremely rapid and spatially localized tissue-resident T-cell response. *Immunol Rev*.

2018;285(1):113–133.

57. Sawtell NM, Thompson RL, Haas RL. Herpes simplex virus DNA synthesis is not a decisive regulatory event in the initiation of lytic viral protein expression in neurons in vivo during primary infection or reactivation from latency. *J Virol*. 2006;80(1):38–50.

58. Schiffer JT, et al. Frequent release of low amounts of herpes simplex virus from neurons: results of a mathematical model. *Sci Transl Med*. 2009;1(7):7ra16.

59. Schiffer JT, Mayer BT, Fong Y, Swan DA, Wald A. Herpes simplex virus-2 transmission probability estimates based on quantity of viral shedding. *J R Soc Interface*. 2014;11(95):20140160.

60. Corey L, et al. Once-daily valacyclovir to reduce the risk of transmission of genital herpes. *N Engl J Med*. 2004;350(1):11–20.

61. Peng T, Zhu J, Phasouk K, Koelle DM, Wald A, Corey L. An effector phenotype of CD8+ T cells at the junction epithelium during clinical quiescence of herpes simplex virus 2 infection. *J Virol*. 2012;86(19):10587–10596.

62. Cunningham AL, Nelson PA, Fathman CG, Merigan TC. Interferon gamma production by herpes simplex virus antigen-specific T cell clones from patients with recurrent herpes labialis. *J Gen Virol*. 1985;66 (pt 2):249–258.

63. Spruance SL, Green JA, Chiu G, Yeh TJ, Wenerstrom G, Overall JC. Pathogenesis of herpes simplex labialis: correlation of vesicle fluid interferon with lesion age and virus titer. *Infect Immun*. 1982;36(3):907–910.

64. Torseth JW, Nickoloff BJ, Basham TY, Merigan TC. Beta interferon produced by keratinocytes in human cutaneous infection with herpes simplex virus. *J Infect Dis*. 1987;155(4):641–648.

65. Kim M, et al. Relay of herpes simplex virus between Langerhans cells and dermal dendritic cells in human skin. *PLoS Pathog*. 2015;11(4):e1004812.

66. Petro C, et al. Herpes simplex type 2 virus deleted in glycoprotein D protects against vaginal, skin and neural disease. *Elife*. 2015;4: e06054.

67. Hufford MM, Kim TS, Sun J, Braciale TJ. Antiviral CD8+ T cell effector activities in situ are regulated by target cell type. *J Exp Med*. 2011;208(1):167–180.

68. Carpenter AE, et al. CellProfiler: image analysis software for identifying and quantifying cell phenotypes. *Genome Biol*. 2006;7(10):R100.

69. Staples E, Ingram RJ, Atherton JC, Robinson K. Optimising the quantification of cytokines present at low concentrations in small human mucosal tissue samples using Luminex assays. *J Immunol Methods*. 2013;394(1-2):1–9.

70. Roychoudhury P, Shrestha N, Wiss VR, Krone SM. Fitness benefits of low infectivity in a spatially structured population of bacteriophages. *Proc Biol Sci*. 2014;281(1774):20132563.